METALS AND MATERIALS International, Vol. 8, No. 4 (2002), pp. 403~410

Bonding Phenomena of Transient Liquid Phase Bonded Joints of a Ni Base Single Crystal Superalloy

Dae-Up Kim and Kazutoshi Nishimoto*

Research Institute, Hyundai MOBIS Co.
80-10 Mabuk-ri, Guseong-eup, Yongin 449-910, Korea
*Department of Manufacturing Science Engineering, Osaka University
2-1 Yamada-oka, Suita, Osaka 565-0871, Japan

The bonding phenomena of Ni base single crystal superalloy CMSX-2 during transient liquid phase (TLP) bonding have been investigated using MBF-80 and F-24 insert metals. TLP bonding of the superalloy was carried out at 1373-1548K for 0-19.6ks in vacuum and the (100) plane of each test specimen was always aligned perpendicular to the joint interface. The dissolution width increased when the bonding temperature and holding time increased. The eutectic width decreased linearly with the square root of holding time during isothermal solidification. After homogenization treatment, the microstructure, distributions of hardness and alloying elements in the bonded interlayer become similar to those of the base metal.

Key words : Ni base single crystal, TLP bonding, dissolution, isothermal solidification, homogenization

1. INTRODUCTION

Ni base single crystal superalloys have excellent mechanical properties at elevated temperatures and have been used as heat-resistant materials [1,2]. In order to apply such single crystal superalloys widely in parts with complicated shapes, it is essential that a new joining technique be developed, maintaining the superior properties of the Ni base single crystal superalloys. The elevated temperature properties of a single crystal will deteriorate when grain boundaries are formed in the joint region. Therefore, it is vital for single crystallization of the bonded region to be achieved during bonding [3].

Several studies on the bonding of Ni base single crystal superalloys have been carried out. In diffusion bonded Ni base single crystal superalloy TMS-26 material, the recrystallization did not occur and the tensile strength of the joints was strongly affected by the twist angle between the bonded materials [4,5]. During the TLP bonding of Ni base single crystal superalloy (Ni-6.6Cr-12.6W-7.6Ta-4.9Al alloy) base metal using MBF-30 filler metal, the solid phase grew epitaxially from the base metal during isothermal solidification, attributed to the dissolution of recrystallized grains at the faying surfaces [6]. When Ni base single crystal (Ni-9.0Cr-10.5W-3.2Ta-5.7Al-3.2Ti-1.0Mo alloy) base material was TLP bonded using Ni-4.1B-2.9Si filler metal, the microconstituents precipitated in the bonded interlayer detrimentally influenced the mechanical properties of the joints [7]. Although several researchers have evaluated the joining characteristics of single crystal superalloys, a detailed examination of the joining process has not been carried out to-date.

The objective of the present study is to develop a reliable bonding technique for single crystal superalloy base material. This paper describes the bonding phenomena of joints produced using TLP bonding.

2. EXPERIMENTAL DETAILS

2.1 Materials

Ni base single crystal superalloy CMSX-2, having the <001> orientation within 8 degrees, was used as the base metal in this study. The orientation of the single crystal was <001> with a bonding face of (100) and it always aligned perpendicular to the joint interface. Two kinds of insert metals, MBF-80 and F-24 (whose chemical composition is similar to CMSX-2 base metal) amorphous foils, were employed as the insert metal. The chemical compositions of the materials are shown in Table 1.

2.2 Experimental Procedure

Using a spark erosion machine, three lines were engraved on the base metal to confirm the original crystal orientation during bonding. The specimens were polished only with 1500 grade emery paper. The insert metal was inserted at the joint

Table 1. Chemical compositions of materials used (mass%)

Materials		B	Cr	Co	Mo	W	Ti	Al	Ta	Ni
Base metal	CMSX-2	-	8.0	4.6	0.6	8.0	1.0	5.6	6.0	Bal.
Insert metal	MBF-80	3.7	15.5	-	-	-	-	-	-	Bal.
	F-24	2.8	8.8	10.8	-	3.7	-	2.9	3.0	Bal.

interface and the orientation of each single crystal specimen matched each other. The specimens were bonded in a vacuum of 13.3 mPa with an applied bonding pressure of 2.3 MPa. The bonding temperature was varied from 1373 to 1548 K, while the holding time was varied from 0-19.6 ks. For the microstructural observation, a 50 μm diameter tungsten spacer was inserted between the contacting substrates and the insert metal (to maintain the constant gap width at the joint interface).

The microstructure of the bonded interlayer was observed using SEM following etching in ethyl alcohol - 10% hydrochloric acid. EDX and EPMA were employed to analyse the chemical compositions near the bonding interface. The dissolution width of the base metals was measured within an area having an 8 mm width from the center of the bonded layer. The dissolution width of the base metal, X, was determined using the following equation [8,9].

$$X = \{(B_1 + B_2) - (S_b - I_b)\}/2 \quad (1)$$

where B_1 and B_2 are the thickness of the base metal before bonding, S_b is the total thickness of the joint after bonding and I_b is the width of the dissolved zone. The average width of the eutectic layer during isothermal solidification was measured by evaluating the eutectic widths at 12 points and at 400 magnification. The dissolution and eutectic widths were evaluated over a distance of 8mm at the mid-section of the bonded specimens.

3. RESULTS AND DISCUSSION

Transient liquid phase (TLP) bonding involves a series of three stages : the base metal dissolution process, the isothermal solidification process and the homogenization process of the constituent elements.

3.1 Base metal dissolution process

The base metal dissolution process during TLP bonding has already been examined based on a derivation of the Nernst-Brunner theory [10].

$$N = Ns[1\text{-}\exp\{-K(S/V)t\}] \quad (2)$$

where N is the solute concentration in the liquid phase, N_s is the saturated concentration of the solute in the liquid phase, K is the dissolution rate constant, S is the area of the solid-liquid interface and V is the volume of the reacted liquid. Differentiating Eq. 2 and assuming that the total amount of the solute in the liquid phase remains constant, the equation for the dissolution reaction between the base metal and the liquid insert metal can be solved by applying an initial condition, X=0 at t=0.

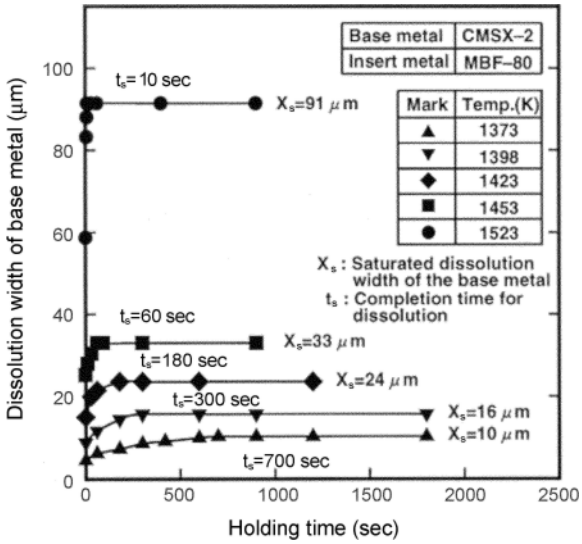

Fig. 1. Effect of the holding time on the dissolution width of the base metal for joints bonded using MBF-80 insert metal.

$$P = Kt = h[ln\{Xs(X+ph)/ph(Xs-X)\}] \quad (3)$$

where P is the dissolution parameter, $2h$ is the initial width of the liquid phase, X is the dissolution width of the base metal after holding time, t, X_s is the saturated dissolution width of the base metal and p is the density ratio of the liquid phase to solid phase.

Fig. 1 shows the effect of holding time on the dissolution width of the base metal at various bonding temperatures for joints bonded MBF-80 insert metal. Base metal dissolution occurs very rapidly and the dissolution width becomes constant at any selected bonding temperature. X_s and t_s in Fig. 1 are the saturated dissolution width of the base metal and the completion time for dissolution at each temperature, respectively. The time required for completing the dissolution at 1523 K was only 10 sec and the liquid width attained the maximum value of 91 μm. The saturated dissolution width of the base metal increased and the completion time for dissolution decreased when the bonding temperature increased.

The relation between the dissolution parameter, P, and the holding time, t, for joints bonded MBF-80 insert metal is shown in Fig. 2. There was a linear relationship between P and t at all bonding temperatures. The slopes of lines (the dissolution rates K) were 0.09, 0.80 and 6.75 at 1373 K, 1453 K and 1523 K, respectively. It follows that the base metal dissolution phenomenon during TLP bonding of sin-

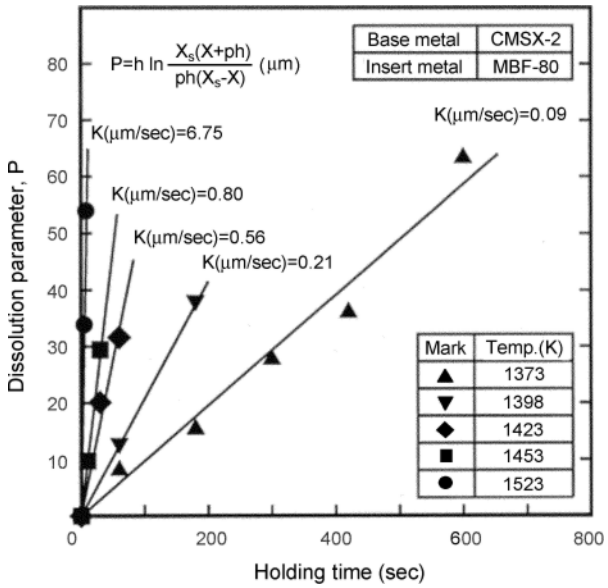

Fig. 2. Relationship between the dissolution parameter and the holding time for joints bonded using MBF-80 insert metal.

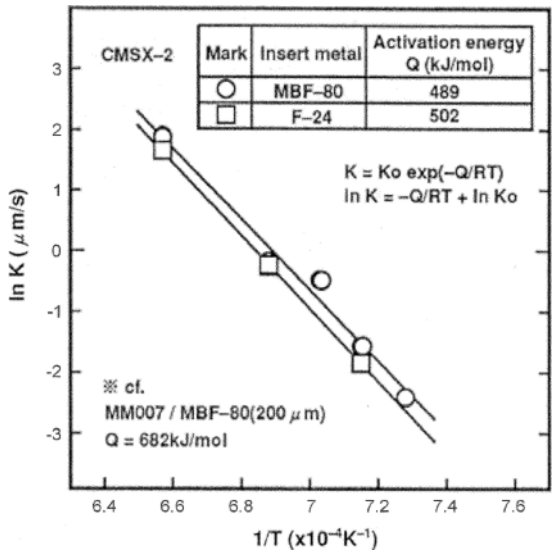

Fig. 3. Arrhenius plots of the dissolution rate for CMSX-2 joints.

gle crystal superalloy CMSX-2 is governed by the Nernst-Brunner equation. Based on the temperature dependence of the dissolution rate, K, (in Fig. 2) the apparent activation energy for base metal dissolution can be obtained using an Arrhenius type Eq. 4 [9].

$$K = K_0 \cdot \exp(-Q/RT) \tag{4}$$

Fig. 3 shows the relation between the reciprocal of the bonding temperature, 1/T, and lnK for joints using MBF-80 and F-24 insert metals. There are linear relationships between

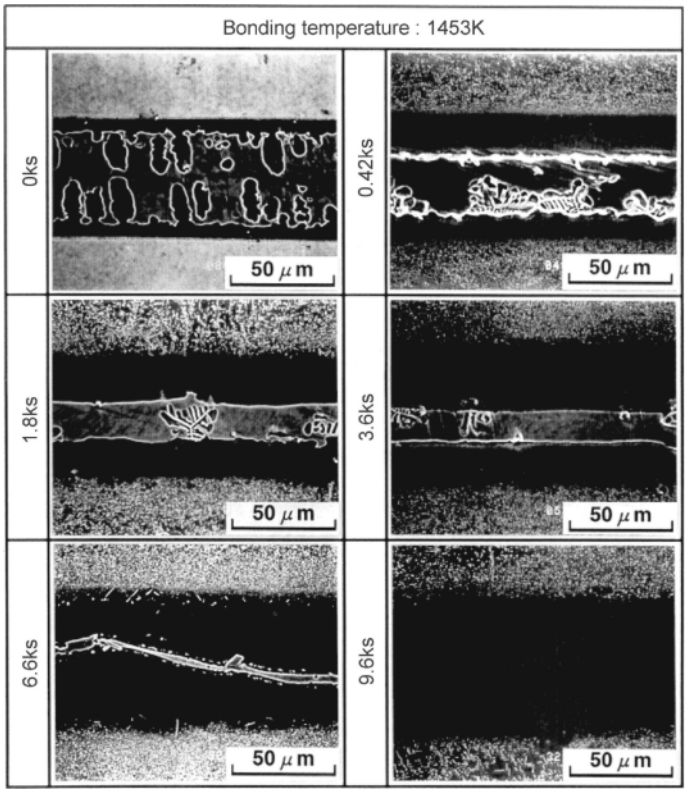

Fig. 4. Change in microstructures of the bonded interlayer with holding time for joints bonded at 1453K using MBF-80 insert metal.

these parameters and the apparent activation energies for base metal dissolution are 502 kJ/mol and 489 kJ/mol for joints using MBF-80 and F-24 insert metals, respectively.

3.2 Isothermal solidification process

Fig. 4 shows the change in microstructures of the bonded interlayer formed during the isothermal solidification with holding time for joints bonded at 1453 K using MBF-80 insert metal. The eutectic width of the bonded interlayer becomes narrower as the holding time increases. Fig. 5 shows the effect of holding time on the eutectic width during the isothermal solidification process for joints bonded MBF-80 insert metal. The eutectic width decreased linearly with the increase in the square root of holding time at the bonding temperature for all joints. The rate of isothermal solidification increased when the bonding temperature increased with the completion time for it at 1523 K being about 1.6 ks. There is not a great difference in the rates of isothermal solidification of CMSX-2 and polycrystal superalloys such as Mar-M247 and Inconel 713 [11].

Assuming that the isothermal solidification process depends on the diffusion of the melting point depressant (boron), the slope of the liquid phase width and holding time relation, m, can be obtained from Fig. 5 using Eq. 5 [12].

$$\ln m = \ln\{(4C_s/V_s\sqrt{\pi})(C_l/V_l - C_s/V_s)^{-1}\} + (1/2)\ln D_0 - Q/2RT \quad (5)$$

where C_s and C_l are the molar ratios of the melting point depressant element in solid and liquid nickel for the chosen alloy system, V_s and V_l are the molar volumes of the solid and liquid phases, Q is the activation energy for diffusion and D_0 and R are constants. Because multicomponent systems were considered in the present study, the C_s and C_l values cannot be derived using equilibrium phase diagrams. Because of this complexity, the assumption that the sum of the first and second terms in Eq. 5 are constant A allows it to be rewritten as the Arrhenius type Eq. 6

$$\ln m = A - Q/2RT \quad (6)$$

Fig. 6 shows the relation between *ln m* and *1/T* for CMSX-2 joints. The results for Ni base polycrystal superalloys such as MM007, Ma-M247, Inconel 713 and Inconel 600 are also indicated in the figure for comparison. The apparent activation energies for isothermal solidification, which correspond to the activation energies for the diffusion of the melting point depressant (boron), are also shown in Table 2. The apparent activation energies for isothermal solidification of CMSX-2 single crystal are 266 kJ/mol (for MBF-80) and 248 kJ/mol (for F-24) and are slightly higher than those found for Ni base polycrystal superalloys (199-219 kJ/mol)

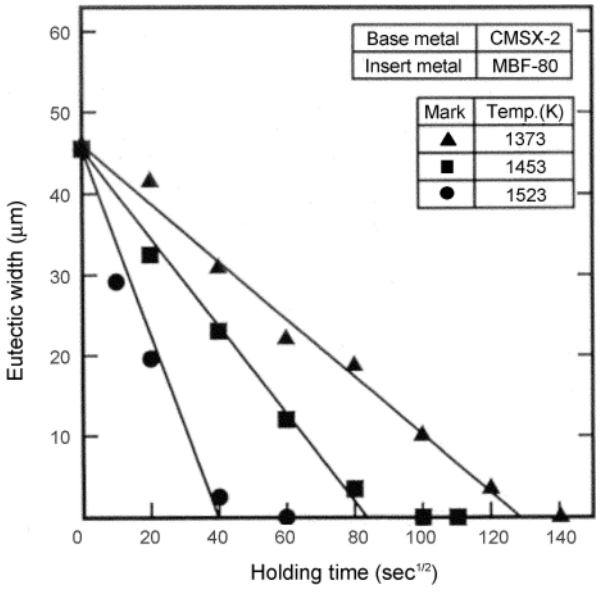

Fig. 5. Relation between the square of the holding time and the eutectic width for joints bonded using MBF-80 insert metal.

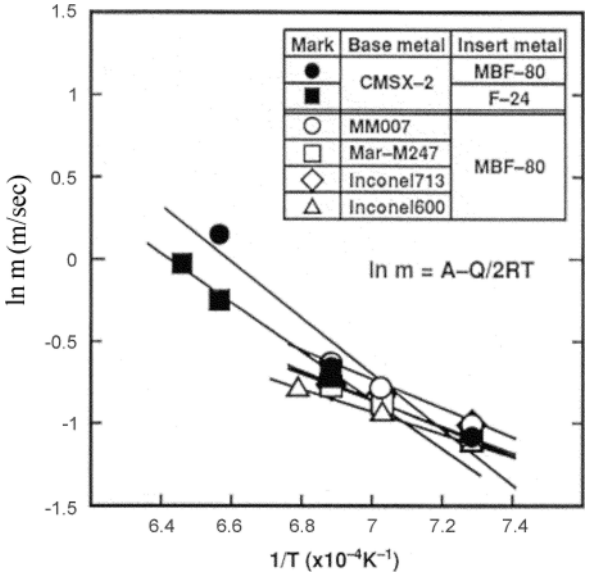

Fig. 6. Arrhenius plots of the isothermal solidification rate for various joints.

Table 2. Activation energies for the isothermal solidification process during the TLP bonding of various Ni base superalloys

Base metal	Insert metal	Bonding temp. (K)	Activation energy (kJ/mol)
CMSX-2	MBF-80	1373-1523	266
	F-24	1453-1548	248
MM 007	MBF-80	1373-1453	219
Mar-M247	MBF-80	1373-1453	199
Inconel 713	MBF-80	1373-1473	211
Inconel 600	MBF-80	1373-1453	209

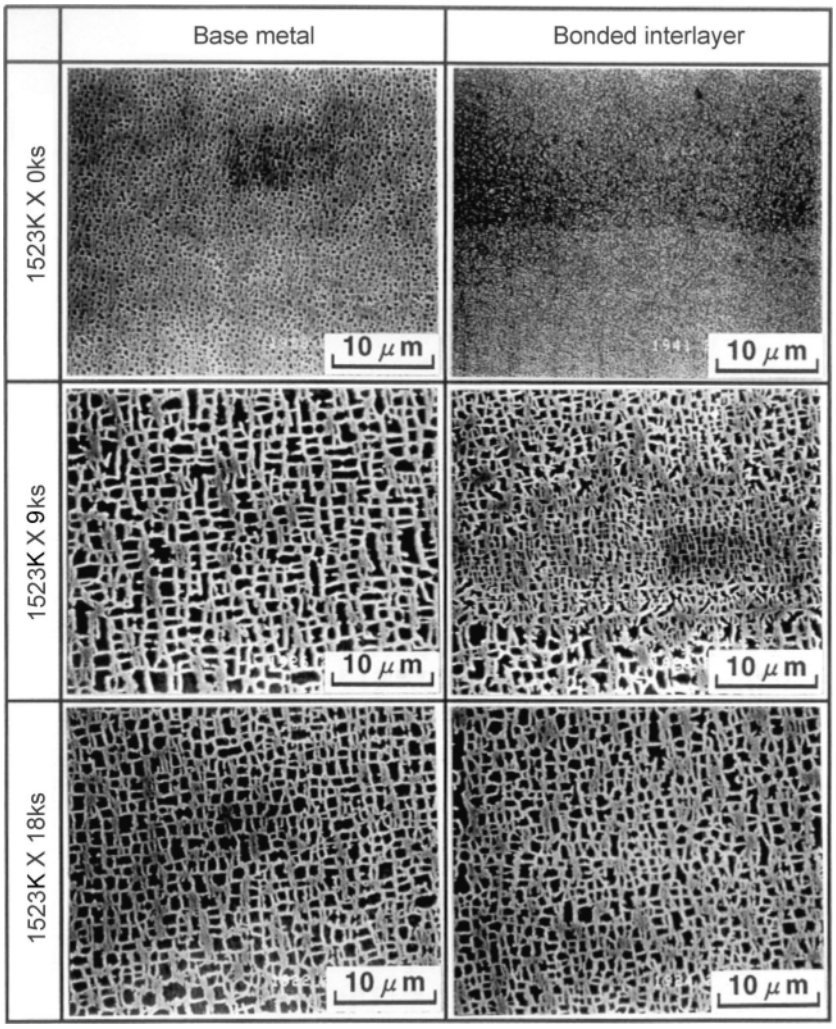

Fig. 7. Microstructures of the bonded interlayer after homogenization treatment for joints bonded using MBF-80 insert metal.

[11]. It has been reported that isothermal solidification is controlled by the diffusion of boron into the base metal in Ni base polycrystal superalloys [11]. The activation energy value found when bonding CMSX-2 base metal would be determined by the diffusion of boron into the solid substrates. In contrast, it is known that grain boundary regions influence the rate of isothermal solidification and that finer grain sizes promote the increased solute diffusion into the base metal [13]. It follows that the difference in activation energies between the single crystal and the polycrystal superalloys base metal can be readily explained by the fact that grain boundary regions can act as high diffusivity paths and these do not exist in single crystal material.

3.3 Homogenization process of the bonded region

It is very important to determine the homogenizing conditions so that the microstructure and concentrations of alloying elements in the bonded interlayer are similar to those of the base metal. Figs. 7 and 8 show the changes in micro-

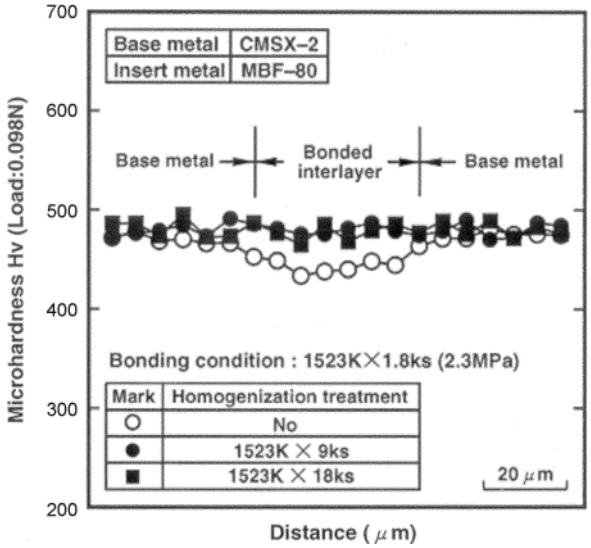

Fig. 8. Microhardness distribution in the bonded interlayer after homogenization treatment for joints bonded using MBF-80 insert metal.

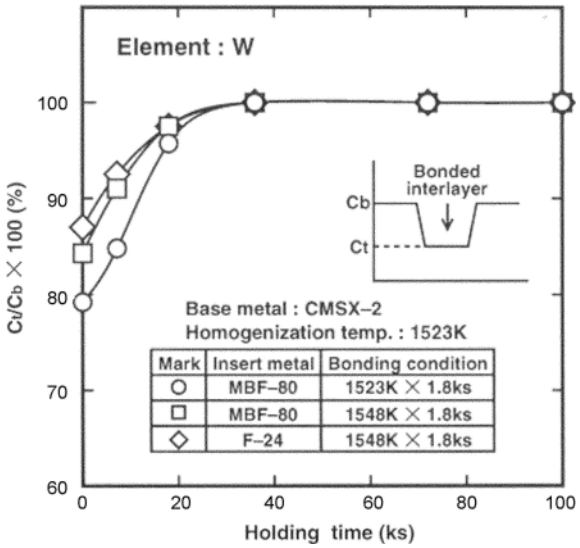

Fig. 9. Effect of homogenization time on the tungsten content at the center of the bonded interlayer.

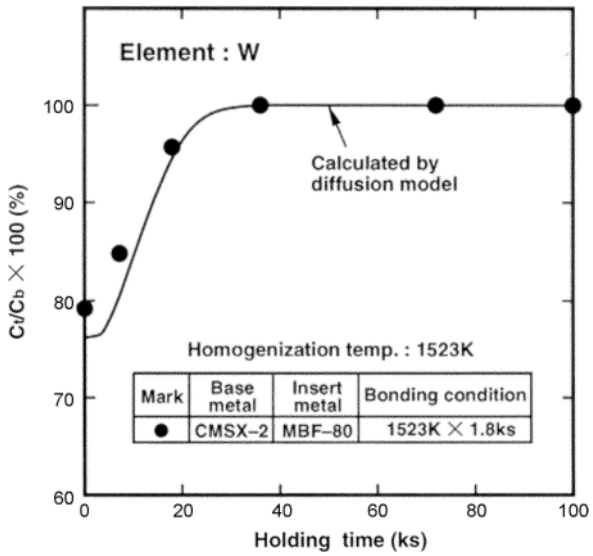

Fig. 10. Effect of the holding time on the tungsten concentration at the center of the bonded interlayer.

structure and microhardness distribution in the bonded interlayer and the base metal with homogenization treatment time for joints following bonding at 1523 K for 1.8 ks, respectively. In the as-bonded joints, the size of phases in the bonded interlayer is smaller than that in the base metal and the hardness in the bonded interlayer is slightly lower than that in the base metal. Both microstructures and microhardness distributions in the bonded interlayer become identical to those in the base metal after the homogenization treatment at 1523 K for 18 ks. The tungsten adjacent to the bonded region was analyzed semi-quantitatively to evaluate the homogenizing behavior following TLP bonding because the diffusivity of tungsten in nickel is deduced to be the slowest of the alloy components [14]. Fig. 9 shows the effect of holding time on the change in the ratio of the tungsten content at the center of the bonded interlayer and that in the base metal of CMSX-2. C_t and C_b in Fig. 9 are the content of tungsten in the bonded interlayer and the base metal, respectively. This content rapidly increased with the increase in holding time at 1523 K and finally approached the concentration level in the base metal. Homogenization of the bonded region was attained earlier when the bonding temperature was increased, and its rate for joints using F-24 insert metal was slightly faster than that for joints using MBF-80 insert metal. It follows that the chemical composition of F-24 filler metal is similar to CMSX-2 base metal.

Nakao *et al.* investigated the homogenization process of alloying elements with a one-dimensional diffusion model and suggested that the concentration of alloying elements in the bonded interlayer, C_t, can be obtained using Eq. 7 in the case when the concentration of alloying elements in the bonded interlayer is of smaller quantity than that of the base metal [15].

$$C_t = C_0[1\text{-}erf\{h/2(Dt)^{1/2}\}]+C_i \quad (7)$$

where C_o: C_b-C_i, C_b is the concentration of the alloying element in the base metal, $2h$ is the initial width of the liquid phase, C_i is the initial concentration of the alloying element in the bonded interlayer and D is the diffusion coefficient of the alloying element. In this study, we compared experimental contents of tungsten at the center of the bonded interlayer with calculated values using Eq. 7. Fig. 10 shows the effect of holding time during the homogenization treatment on the tungsten concentration at the center of the bonded interlayer for joints bonded at 1523 K for 1.8 ks using MBF-80 filler metal. In this calculation, the diffusion coefficient of tungsten in the nickel, $D=1.90\times10^{-4}\exp(-299000/RT)(m^2/sec)$, was used as a diffusion coefficient of tungsten in the CMSX-2 [14]. The initial concentration of tungsten in the bonded interlayer was calculated with Eq. 8, using the dissolution width of the base metal at the completion of its dissolution reaction.

$$C_i = \{(W_B\text{-}W_S)\cdot C_b + W_S\cdot C_{IM}\}/W_B \quad (8)$$

where W_B is the dissolution width of the base metal after holding time, t, W_S is the diameter of the spacer and C_{IM} is the initial concentration of the alloying element in the insert metal. The experimental values of tungsten concentration at the center of the bonded interlayer are more or less higher than the calculated values in the early stage of the homogenization treatment. As the homogenization time increases gradually, experimental values are close to the calculated values. It follows that the calculated value of tungsten concentration using the one-dimensional diffusion model, Eq. 7, is in accord with the experimental value. In the early stage of the diffusion model, it is supposed that the concentration value of tungsten

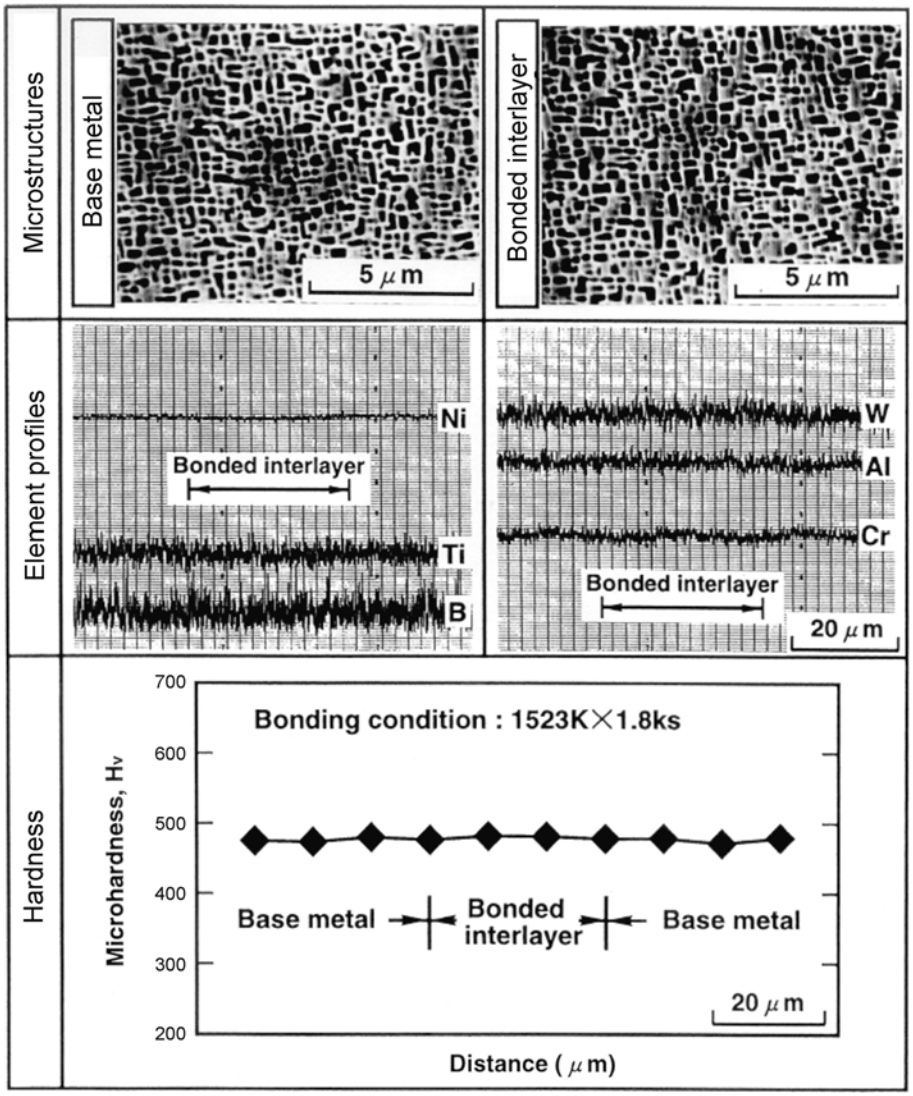

Fig. 11. Microstructures, line profiles of elements and the hardness distribution in the bonded interlayer after solution and aging treatments.

at the center of the bonded interlayer is zero; a slight difference between experimental and calculated values is shown [15].

The microstructures, microhardness distributions and alloying elements in the bonded region of the joint following solution treatment (1589 K×7.2 ks) and the two-step aging treatments (1343 K×14.4 ks×1144 K×72 ks) without any homogenization treatments were also investigated, because the solution treatment and the following aging treatments were indispensable for the following TLP bonding of CMSX-2 base material. The size and shape of phases in the bonded interlayer are similar to those in the base metal. The distributions of microhardness and alloying elements in the bonded interlayer become similar to the base metal substrates as shown in Fig. 11. It follows that joint homogenization takes place during the solution treatment and that the homogenization treatment is not always required during TLP bonding operations.

4. CONCLUSIONS

Bonding phenomena of transient liquid phase bonded Ni base single crystal superalloy CMSX-2 were examined. The principal conclusions can be summarized as follows.

(1) The dissolution width of the base metal increased when the bonding temperature and holding time increased. Base metal dissolution was consistent with a derivation based on the Nernst-Brunner theory. The apparent activation energies for base metal dissolution were 502 kJ/mol (for MBF-80) and 489 kJ/mol (for F-24).

(2) During isothermal solidification, the eutectic width decreased linearly with the increase in the square root of holding time. The apparent activation energies for isothermal solidification were 266 kJ/mol (for MBF-80) and 248 kJ/mol (for F-24) and were higher than those previously reported in Ni base poly-

crystal superalloys.

(3) The microstructure, hardness distribution and alloying elements in the bonded interlayer become identical to those in the base metal after the homogenization treatment at 1523 K for 18 ks. The homogenization of the bonded region was achieved during the solution treatment and homogenization treatment is not always required during TLP bonding operations.

REFERENCES

1. A. D. Cetel and D. N. Duhl, *Proc. of the Int. Symp. on Superalloys 1988*, p. 235, AIME, Pennsylvania, USA (1988).
2. T. Ohno and R. Watanabe, *Tetsu-to-Hagane* **77**, 832 (1991).
3. D. U. Kim, *J. Kor. Inst. Met. & Mater.* **39**, 712 (2001).
4. O. Ohashi and S. Suga, *J. Jpn. Weld. Soc.* **10**, 53 (1992).
5. O. Ohashi, S. Meguro, and T. Yamagata, *J. Jpn. Inst. Met.* **59**, 319 (1995).
6. S. Kamohara, T. Funamoto, K. Yasuda, A. Yoshinari, and T. Shibayanagi, *Proc. of the 3rd Int. Conf. on Trends in Weld. Res.* (eds., S. A. David and J. M. Vitek) p. 1089, ASM Int., Gatlinburg, Tennessee, USA (1992).
7. T. Hirane, A. Yoshinari, and S. Morimoto, *Tetsu-to-Hagane* **72**, s1607 (1986).
8. Y. Nakao, K. Nishimoto, K. Shinozaki, C. Kang, and Y. Hori, *J. Jpn. Weld. Soc.* **6**, 519 (1988).
9. D. U. Kim, C. Y. Kang, and W. J. Lee, *Metals and Materials* **5**, 477 (1999).
10. E. A. Moelwyn-Hughes, *Dissolution in Metals*, p. 374, Claredon Press, Oxford (1974).
11. Y. Nakao, K. Nishimoto, K. Shinozaki, and C. Kang, *J. Jpn. Weld. Soc.* **6**, 67 (1988).
12. Y. Nakao, K. Nishimoto, K. Shinozaki, and C. Kang, *J. Jpn. Weld. Soc.* **7**, 47 (1989).
13. K. Saida, Y. Zhou, and T. H. North, *J. Mater. Sci.* **28**, 6427 (1993).
14. *Kinzoku-Data Book*, p. 27, Maruzen Press, The Jpn. Inst. Metals (1984).
15. Y. Nakao, K. Nishimoto, K. Shinozaki, C. Kang, and H. Shigeta, *J. Jpn. Weld. Soc.* **9**, 55 (1991).